Search for Di-Higgs Production at 13 TeV in ATLAS

David Kirchmeier
on behalf of the ATLAS collaboration

40th International Conference on High Energy Physics ICHEP 2020

ATLAS EXPERIMENT

ErUM-FSP T02 ATLAS

INSTITUTE OF NUCLEAR AND PARTICLE PHYSICS

TECHNISCHE UNIVERSITÄT DRESDEN

Search for Di-Higgs Production

- Di-Higgs final states give access to:
  - **Standard Model (SM)**
  - Anomalous couplings
  - Beyond-the-Standard-Model (BSM) resonances

$$\mathcal{L} = -\tfrac{1}{4} F_{\mu\nu} F^{\mu\nu} + i\bar{\psi}\not{D}\psi + \psi_i y_{ij} \psi_j \phi + \text{h.c.} + |D_\mu \phi|^2 - V(\phi)$$

$$V(\phi) = -\mu^2\phi^2 + \lambda\phi^4$$

- SM predicts trilinear Higgs self-coupling λ^{HHH}
- Direct probe of electroweak symmetry breaking potential
- HH cross section very small: 31 fb at 13 TeV
  due to destructive interference of top quark loop
  with Higgs self-coupling diagram
- Major goal of HL-LHC to measure HH cross section
  and trilinear self-coupling

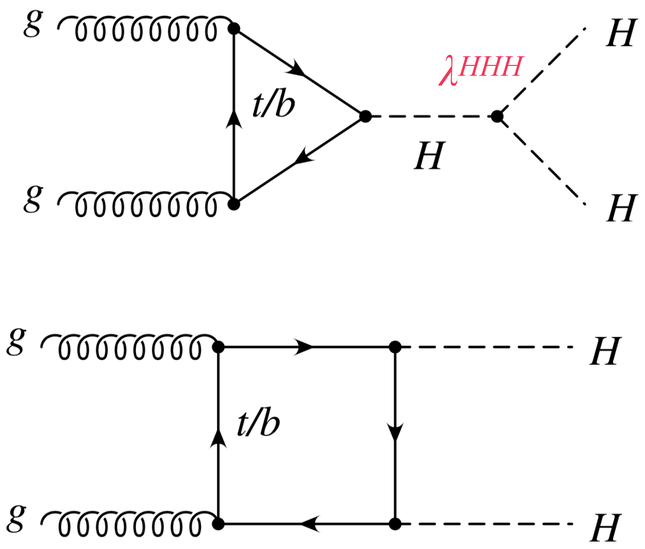

Search for Di-Higgs Production

- Di-Higgs final states give access to:
  - Standard Model (SM)
  - **Anomalous couplings**
  - Beyond-the-Standard-Model (BSM) resonances

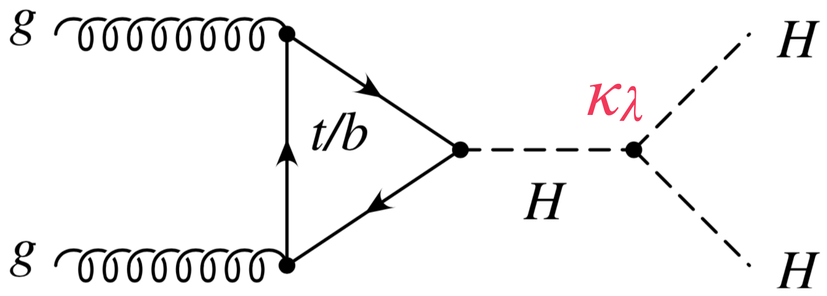

- Sensitive to anomalous deviations of the coupling strength $\kappa_\lambda = \lambda^{HHH} / \lambda_{SM}^{HHH}$ already in Run 2
- κ_λ has large impact on cross section and kinematics

JHEP06(2019)066

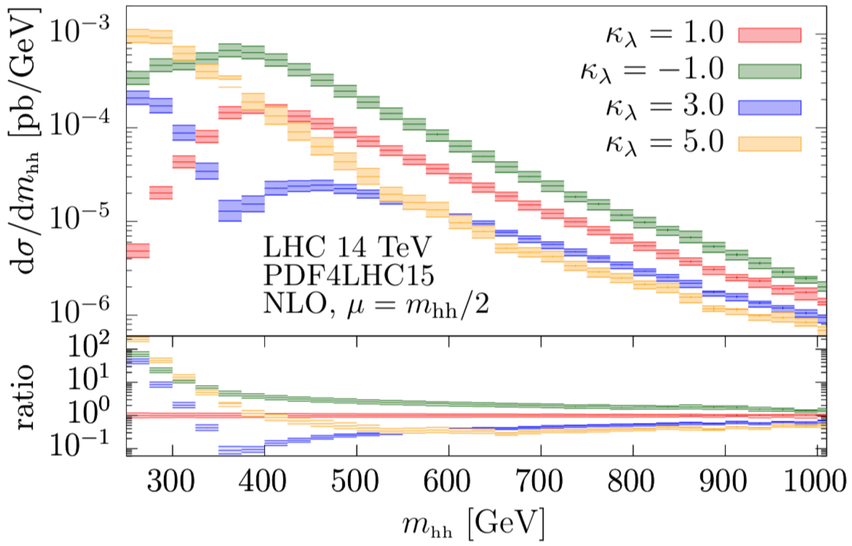

Search for Di-Higgs Production

- Di-Higgs final states give access to:
  - Standard Model (SM)
  - Anomalous couplings
  - **Beyond-the-Standard-Model (BSM) resonances**

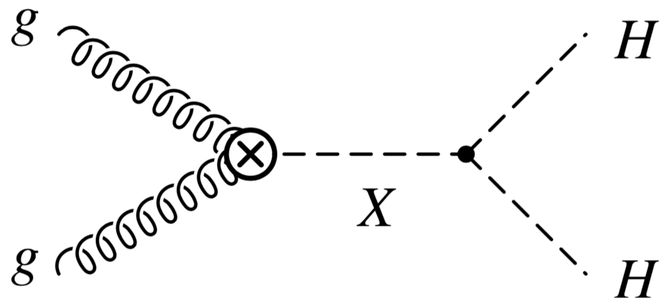

- Several BSM models predict existence of heavy particles decaying into 2 Higgs bosons
- Spin-0 resonance: predicted by Two-Higgs-Doublet Models (e.g. MSSM) and Electroweak Singlet Models
- Spin-2 resonance: Kaluza-Klein graviton, predicted in the Randall-Sundrum model of warped extra dimensions

Di-Higgs Final States

Di-Higgs branching ratios

	bb	WW	ττ	ZZ	γγ
bb	34%				
WW	25%	4.6%			
ττ	7.3%	2.7%	0.39%		
ZZ	3.1%	1.1%	0.33%	0.07%	
γγ	0.26%	0.10%	0.03%	0.01%	0.0005%

published by ATLAS

- Variety of final states
- H→bb: highest BR
- Leptonic final states:
  high background suppression
- Production modes:

gluon-gluon fusion (ggF)

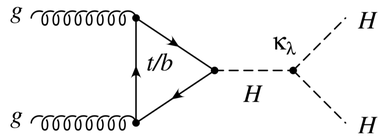

vector boson fusion (VBF)

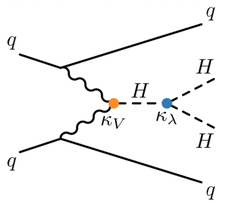

- Topology of decay products:

resolved

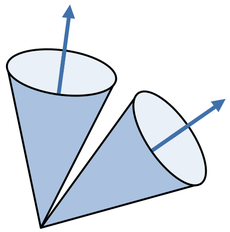

boosted

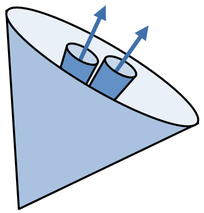

Di-Higgs Final States

Channel	L [fb^{-1}]	Production	Decay	Reference
bbbb	36	ggF	resolved + boosted	JHEP 01 (2019) 030
bbbb	**127**	**VBF**	**resolved**	**JHEP 07 (2020) 108**
bbWW->bblvqq	36	ggF	resolved + boosted	JHEP 04 (2019) 092
bb(WW/ZZ/ττ)->bblvlv	**139**	**ggF**	**resolved**	**Phys. Lett. B 801 (2020) 135145**
bbττ	36	ggF	resolved	Phys. Rev. Lett. 121 (2018) 191801
bbττ	**139**	**ggF**	**boosted**	**arXiv:2007.14811**
WWWW->lvlv(lvlv / lvqq / qqqq)	36	ggF	resolved	JHEP 05 (2019) 124
bbγγ	36	ggF	resolved	JHEP 11 (2018) 040
γγWW->γγlvjj	36	ggF	resolved	Eur. Phys. J. C 78 (2018) 1007

Di-Higgs Production

Phys. Lett. B 800 (2020) 135103

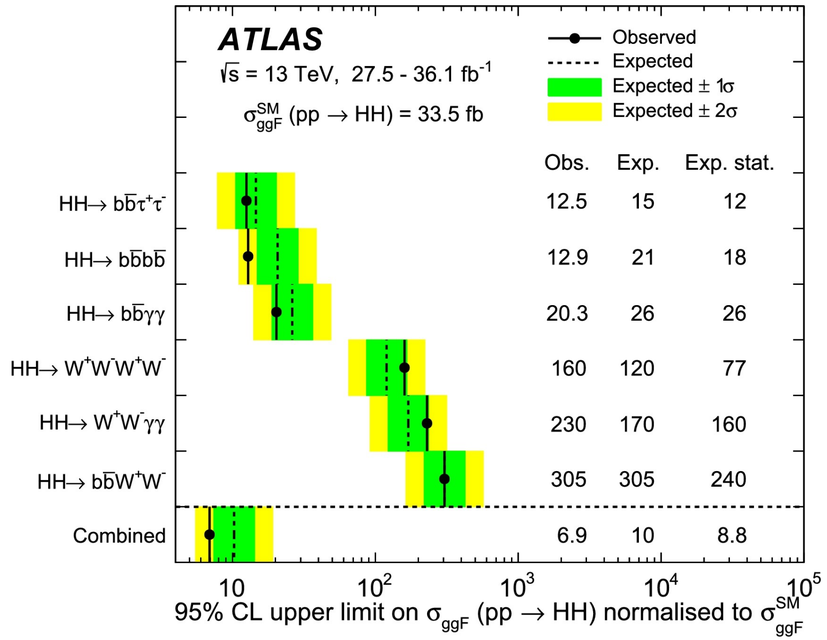

- Combination of searches for Higgs boson pair production using up to 36.1 fb^{-1}

Di-Higgs Production

Phys. Lett. B 800 (2020) 135103

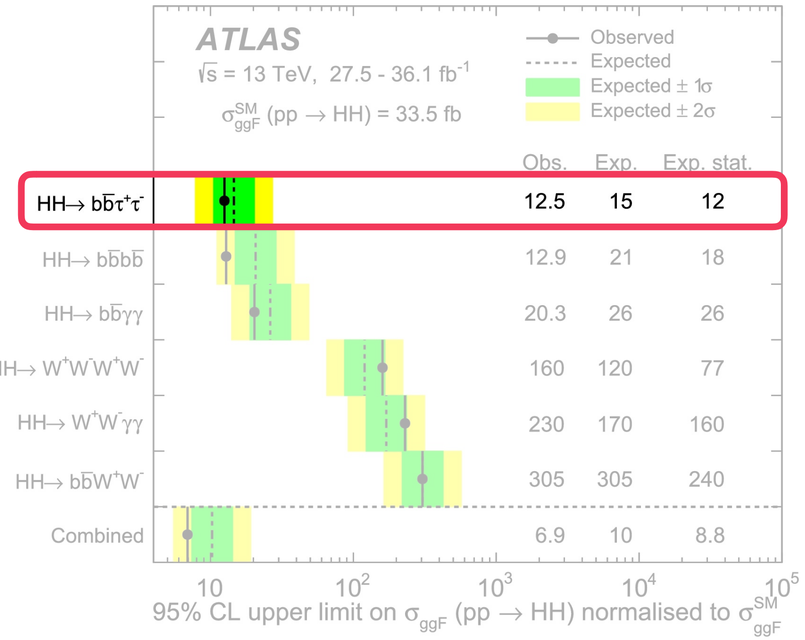

- Combination of searches for Higgs boson pair production using up to 36.1 fb^{-1}

bbττ Final State

- Two b-tagged (R=0.4) jets
- Two τ-leptons ($\tau_{had}\tau_{had}$ or $\tau_{lep}\tau_{had}$)
- Triggers: τ_{had}, $\tau_{had}+\tau_{had}$, ℓ, $\ell+\tau_{had}$
- Boosted decision tree (BDT) as final discriminant

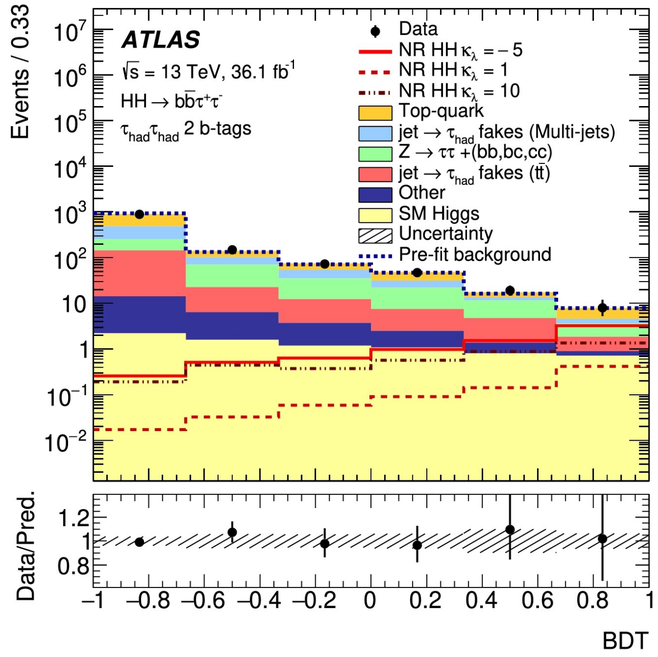

Di-Higgs Production

Phys. Lett. B 800 (2020) 135103

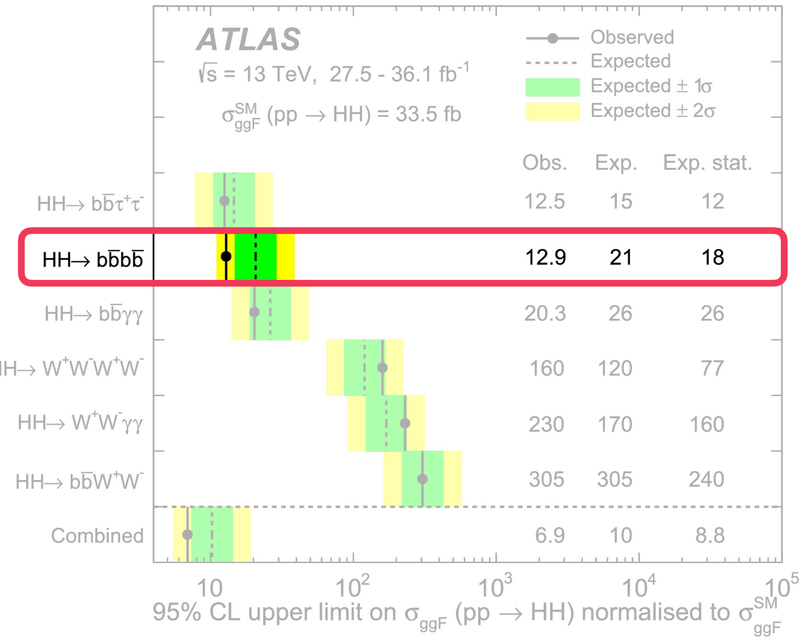

- Combination of searches for Higgs boson pair production using up to 36.1 fb^{-1}

bbbb Final State

- Resolved analysis:
  four (R=0.4) jets, each b-tagged
- Boosted analysis:
  two (R=1.0) jets, each with 1 or 2 b-tagged (R=0.2) track jets inside
- m_{HH} as final discriminant

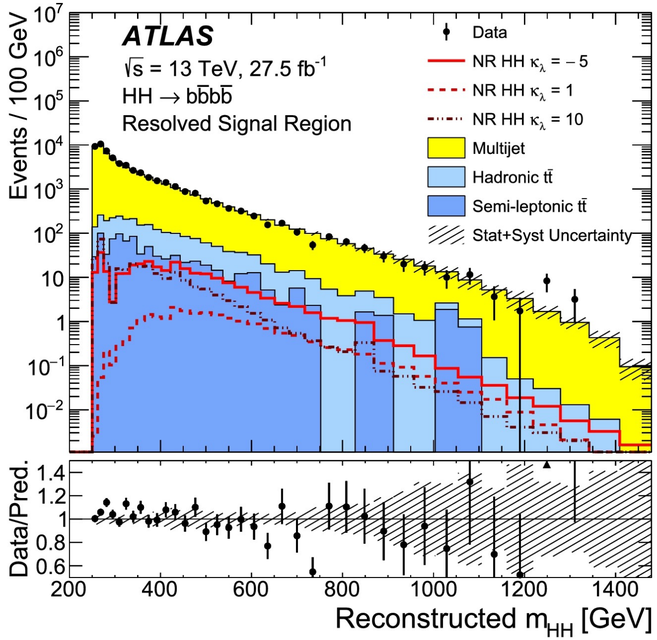

Di-Higgs Production

Phys. Lett. B 800 (2020) 135103

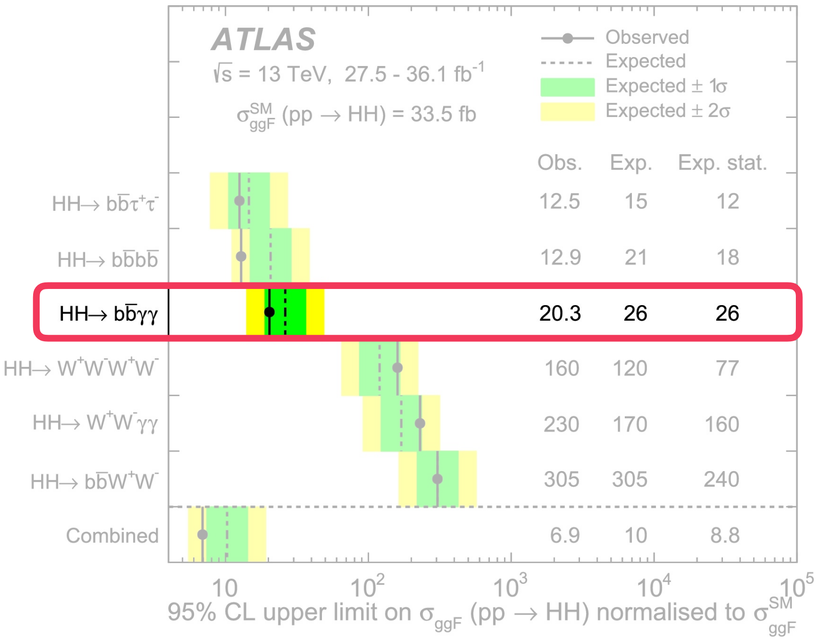

- Combination of searches for Higgs boson pair production using up to 36.1 fb^{-1}

bbγγ Final State

- One or two b-tagged (R=0.4) jets and two high-p_T isolated photons
- Two different jet p_T selections for non-resonant and resonant searches

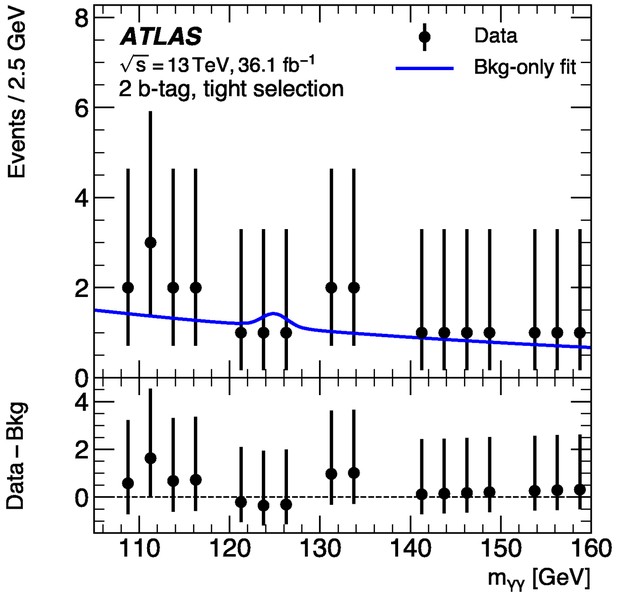

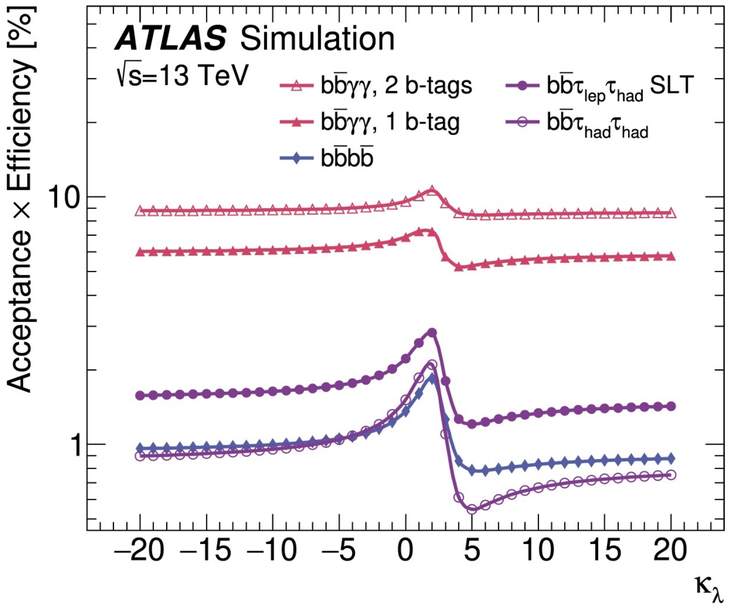

Di-Higgs Production

Phys. Lett. B 800 (2020) 135103

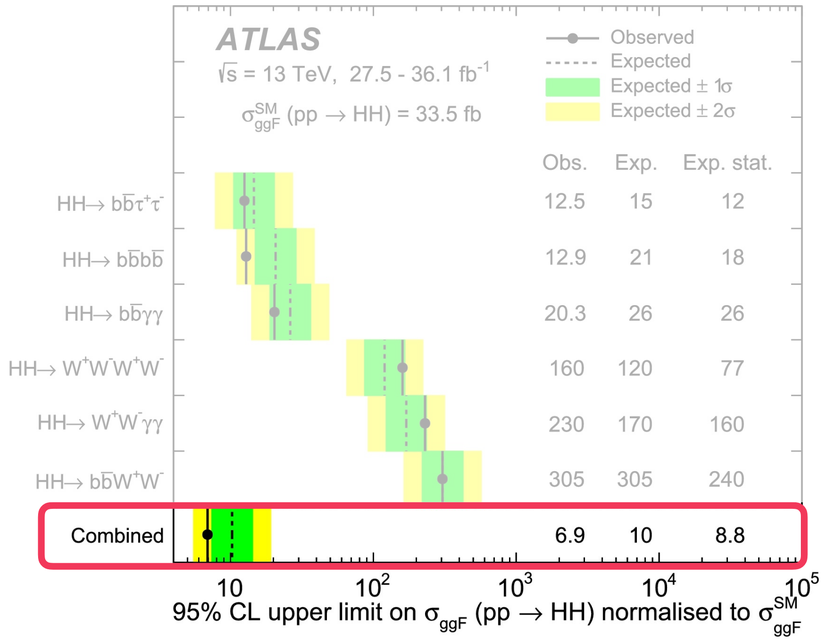

- Combination of searches for Higgs boson pair production using up to 36.1 fb^{-1}

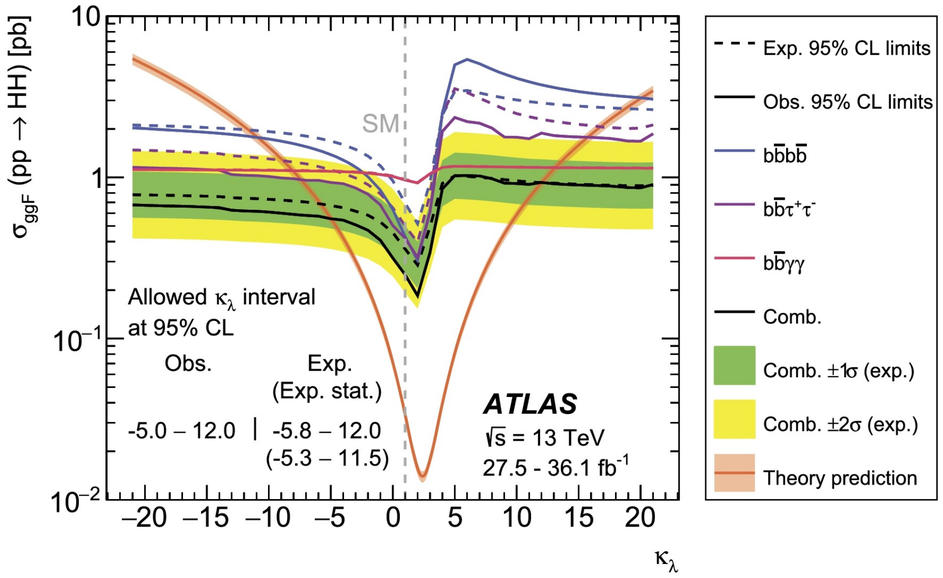

- Production cross-section obs. (exp.) limit: 6.9 (10) times the SM prediction
- Constraints on κ_λ obs. (exp.): $-5.0\ (-5.8) < \kappa_\lambda < 12.0\ (12.0)$

Di-Higgs Production

Phys. Lett. B 800 (2020) 135103

- Limits are set on the production of:
  - Narrow scalar resonances
  - Spin-2 Kaluza-Klein gravitons
- In the parameter space of:
  - habemus MSSM? (hMMSM)
  - Electroweak Singlet Model

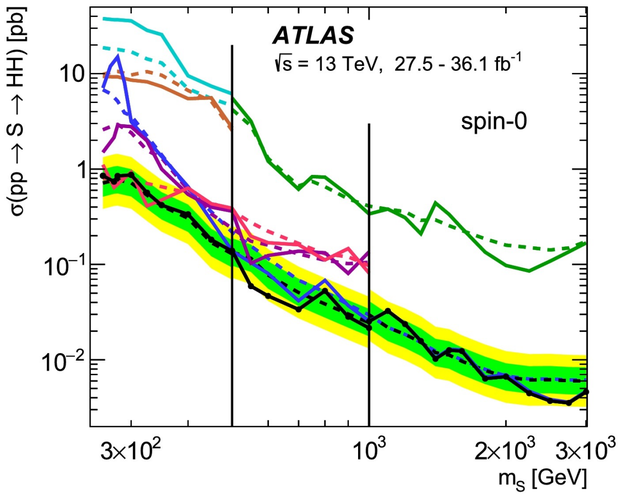

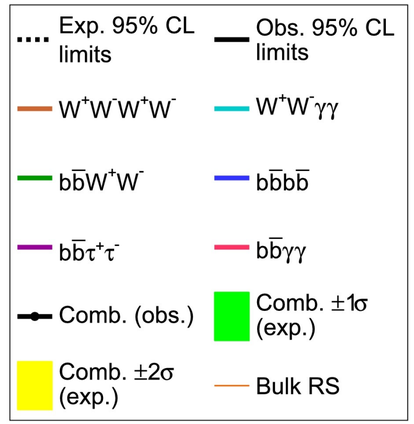

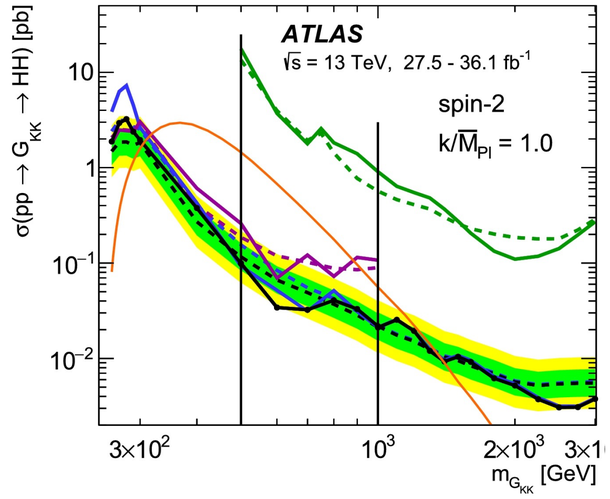

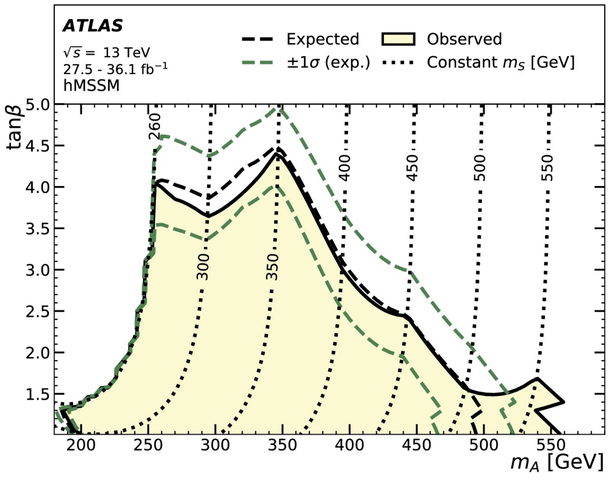

Vector Boson Fusion HH→bbbb

Full Run 2 Dataset!

JHEP 07 (2020) 108

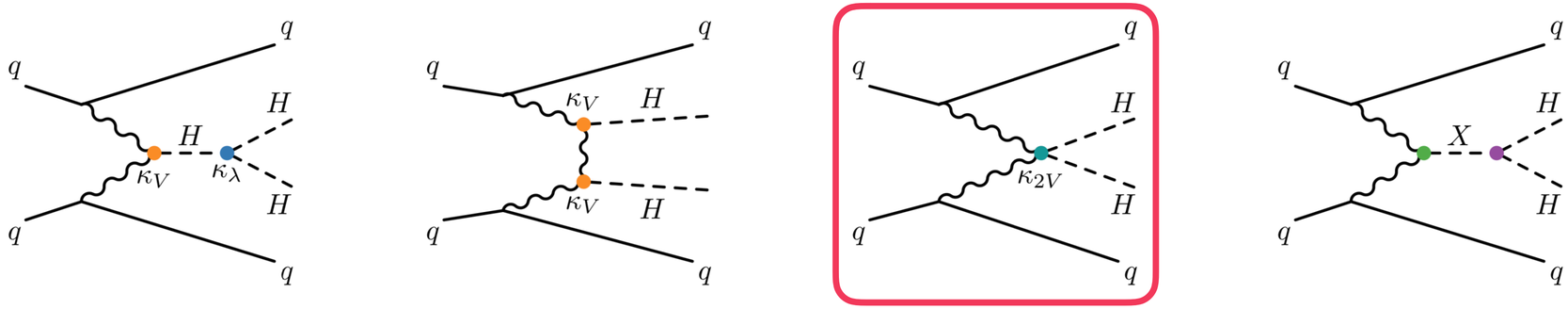

- First look at di-Higgs production via vector boson fusion
- Distinct event topology with 4 central b-tagged jets and two high-p_T forward jets
- Multi-jet background estimated from data events with lower b-jet multiplicity
- Obs. (exp.) limit on σ_{VBF}^{HH}: 840 (550) times SM
- Constrains quartic coupling between Higgs and vector bosons obs (exp): -0.76 (-0.91) < κ_{2V} < 2.90 (3.11)

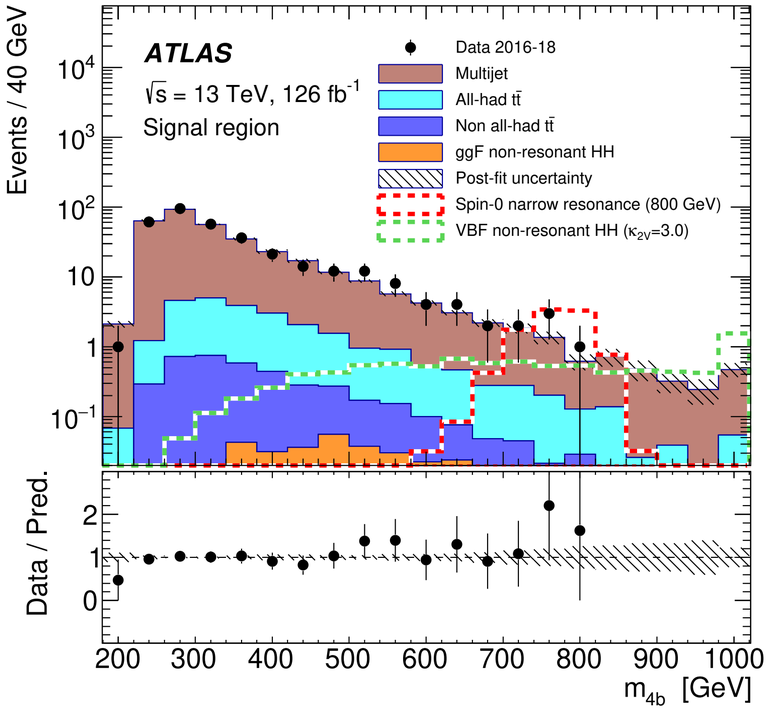

Vector Boson Fusion HH→bbbb

Full Run 2 Dataset!

JHEP 07 (2020) 108

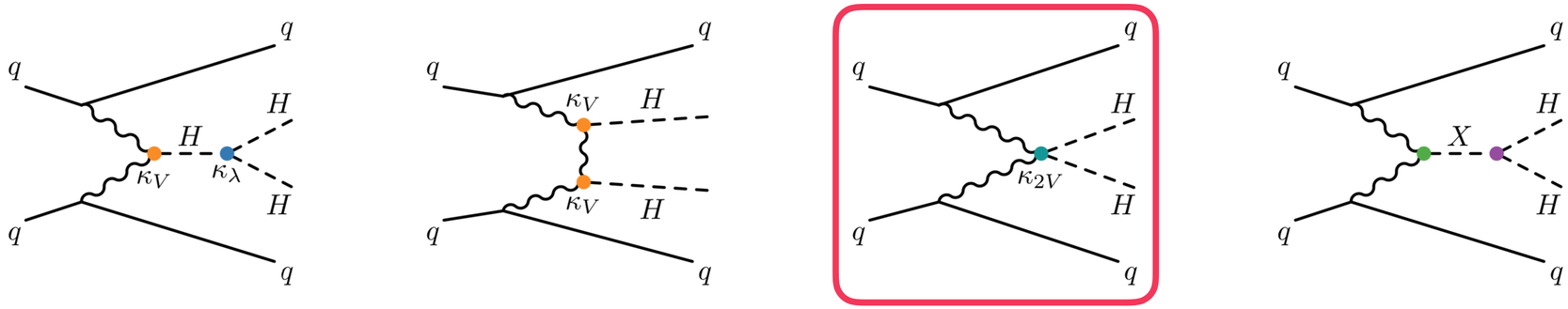

- First look at di-Higgs production via vector boson fusion
- Distinct event topology with 4 central b-tagged jets and two high-p_T forward jets
- Multi-jet background estimated from data events with lower b-jet multiplicity
- Obs. (exp.) limit on σ_{VBF}^{HH}: 840 (550) times SM
- Constrains quartic coupling between Higgs and vector bosons obs (exp): -0.76 (-0.91) < κ_{2V} < 2.90 (3.11)

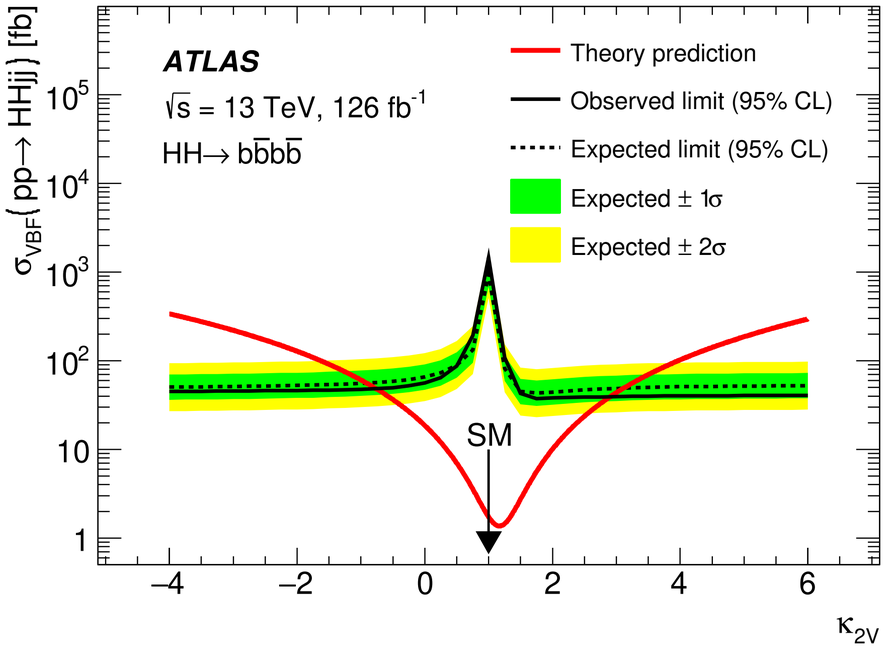

bbℓνℓν Final State

Full Run 2 Dataset!

Phys. Lett. B 801 (2020) 135145

- First search for SM di-Higgs production via gluon-gluon fusion with full Run 2
- H→bb and H→WW/ZZ/ττ
- Two b-tagged jets and two electrons or muons with opposite electric charge
- Deep neural network classifier, $m_{\ell\ell}$ and m_{bb} cuts
- Obs. (exp.) limit on σ_{ggF}^{HH}: 40 (29) times SM

	-2σ	-1σ	Expected	$+1\sigma$	$+2\sigma$	Observed
$\sigma\,(gg \to HH)$ [pb]	0.5	0.6	0.9	1.3	1.9	1.2
$\sigma\,(gg \to HH)\,/\sigma^{\mathrm{SM}}\,(gg \to HH)$	14	20	29	43	62	40

$$d_{HH} = \ln\left[p_{HH}/(p_{\mathrm{Top}} + p_{Z-\ell\ell} + p_{Z-\tau\tau})\right]$$

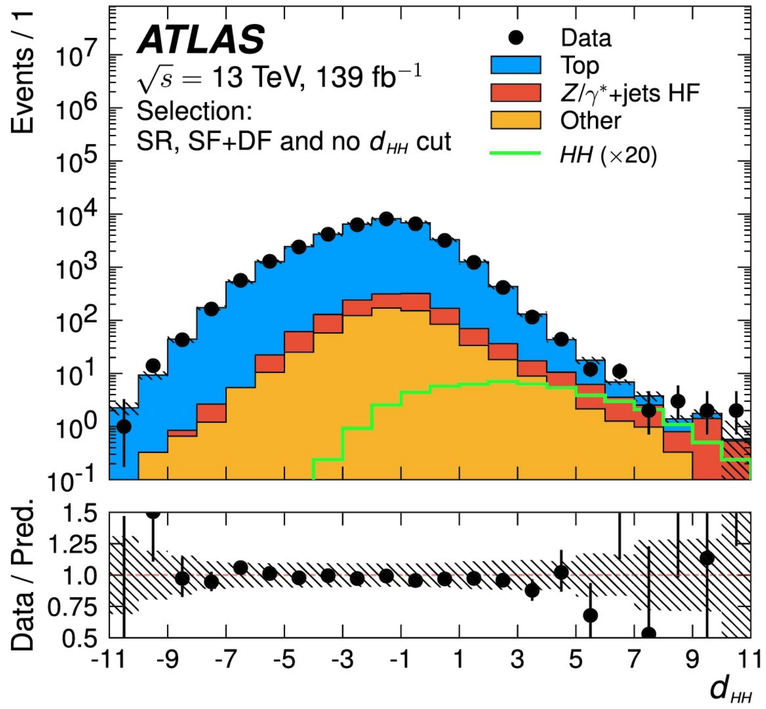

Boosted bbττ Final State

Full Run 2 Dataset!

arXiv:2007.14811

- Novel technique to reconstruct boosted tau pairs is employed for first time in an ATLAS search
- Pair of τ_{had} decays reconstructed as (R=1.0) jet with (R=0.2) sub-jets
- Boosted decision tree applied to reject background of quark/gluon-initiated jets
- H→bb candidate contained in (R=1.0) jet, associated track-jets for b-tagging
- Setting limits on production cross section of heavy narrow scalar resonance X

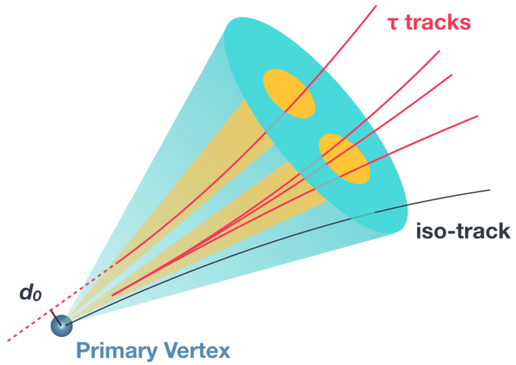

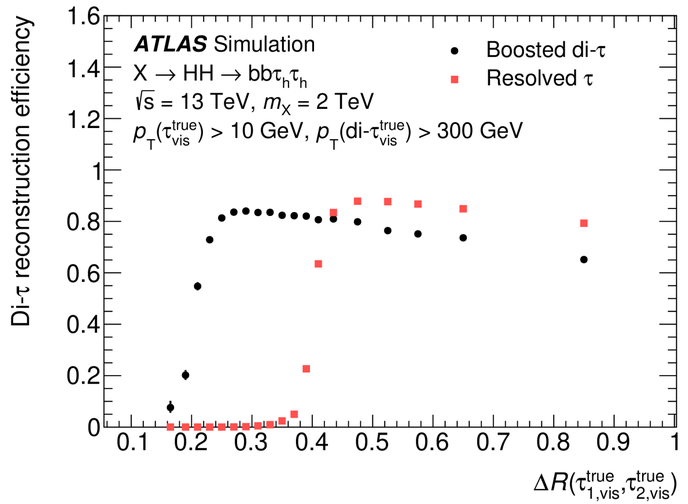

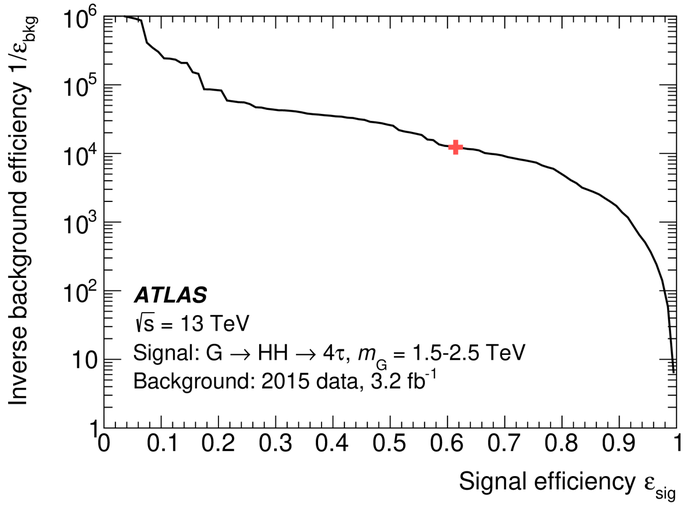

Boosted bbττ Final State

Full Run 2 Dataset!

arXiv:2007.14811

- Novel technique to reconstruct boosted tau pairs is employed for first time in an ATLAS search
- Pair of τ_{had} decays reconstructed as (R=1.0) jet with (R=0.2) sub-jets
- Boosted decision tree applied to reject background of quark/gluon-initiated jets
- H→bb candidate contained in (R=1.0) jet, associated track-jets for b-tagging
- Setting limits on production cross section of heavy narrow scalar resonance X

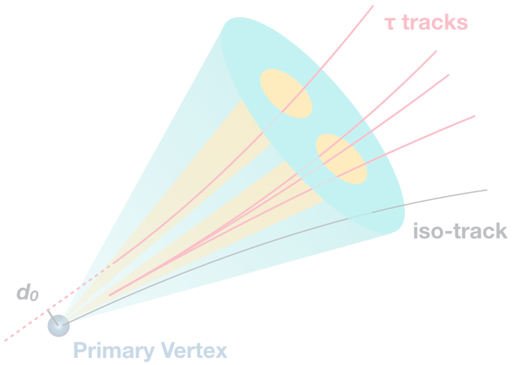

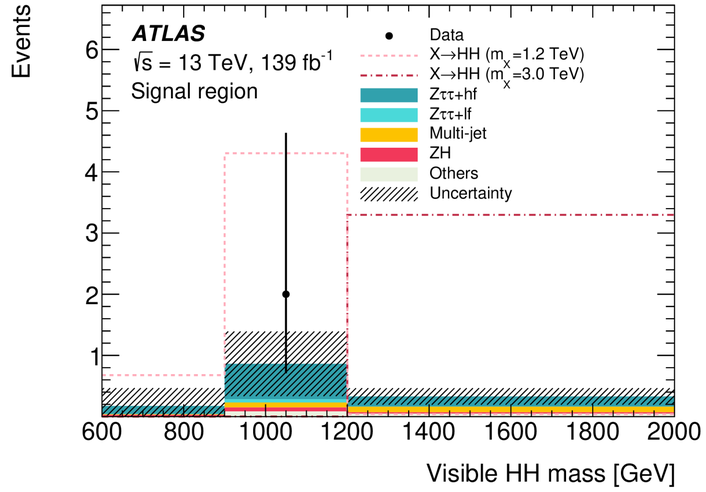

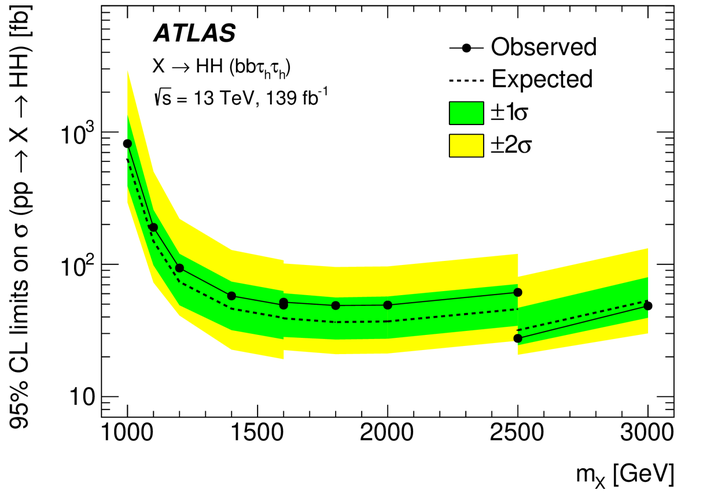

Summary

- **Di-Higgs signatures: key for better understanding of electroweak symmetry breaking**
- Strongest constraints on di-Higgs production from early Run 2 combination
- Upper limit on cross-section at 6.9 x SM (10 x SM expected),
  $-5.0 < \kappa_\lambda < 12.0$
- Looking forward to see this updated with full Run 2 dataset, potentially discovering new physics or further constraining SM couplings
- New channels are explored, like VBF production, bb$\ell\nu\ell\nu$ or boosted bb$\tau\tau$ final states

Additional Material

Di-Higgs Combination

Phys. Lett. B 800 (2020) 135103

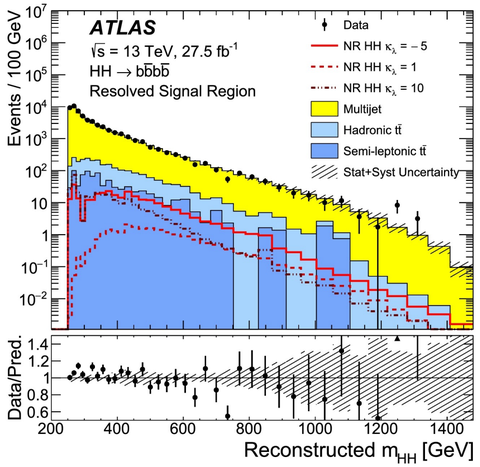

(a)

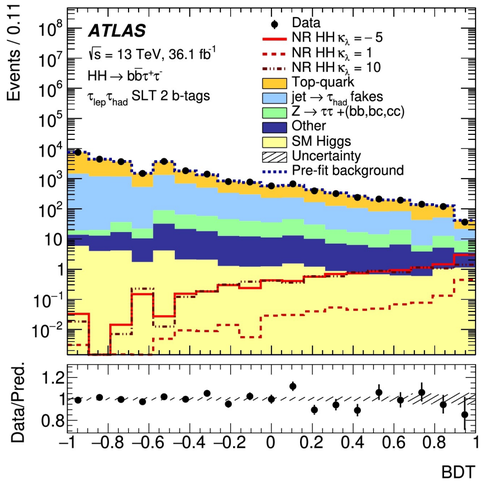

(b)

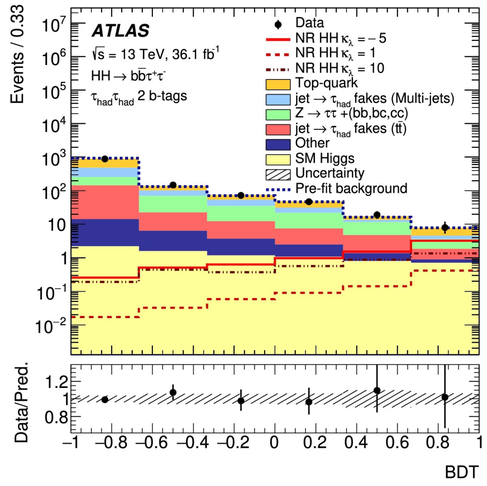

(c)

Fig. 3. Final discriminants used in the κ_λ-scan analysis for the $b\bar{b}b\bar{b}$ and the $b\bar{b}\tau^+\tau^-$ final states. (a) shows the reconstructed m_{HH} distribution in the $b\bar{b}b\bar{b}$ analysis; backgrounds include data-driven multi-jet processes (Multijet), $t\bar{t} \rightarrow W^+W^-b\bar{b}$ with both W bosons decaying hadronically (Hadronic $t\bar{t}$) and $t\bar{t} \rightarrow W^+W^-b\bar{b}$ with at least one of the W bosons decaying leptonically (Semileptonic $t\bar{t}$). (b) and (c) show the BDT distributions in the $b\bar{b}\tau^+\tau^-$ analysis for the $\tau_{\text{lep}}\tau_{\text{had}}$ and the $\tau_{\text{had}}\tau_{\text{had}}$ channels, respectively. The main backgrounds are $t\bar{t}$ and single-top-quark production (Top-quark), the background arising from jets faking hadronic τ-lepton decays (jet→τ_{had} fakes), $Z\rightarrow\tau^+\tau^-$ plus two heavy-flavour jets [$Z\rightarrow\tau\tau$+(bb,bc,cc)], SM single Higgs boson production (SM Higgs) and other minor backgrounds (Other). The shaded area includes the systematic uncertainty of the total background expectation due to the statistics of simulated events and all experimental and theoretical systematic uncertainties. In figures (b) and (c) the uncertainty band is not shown in the upper panes because it is too small to be seen. The signal distribution is overlaid for κ_λ=−5,1,10 and is normalised to its expected yield.

Di-Higgs Combination

Phys. Lett. B 800 (2020) 135103

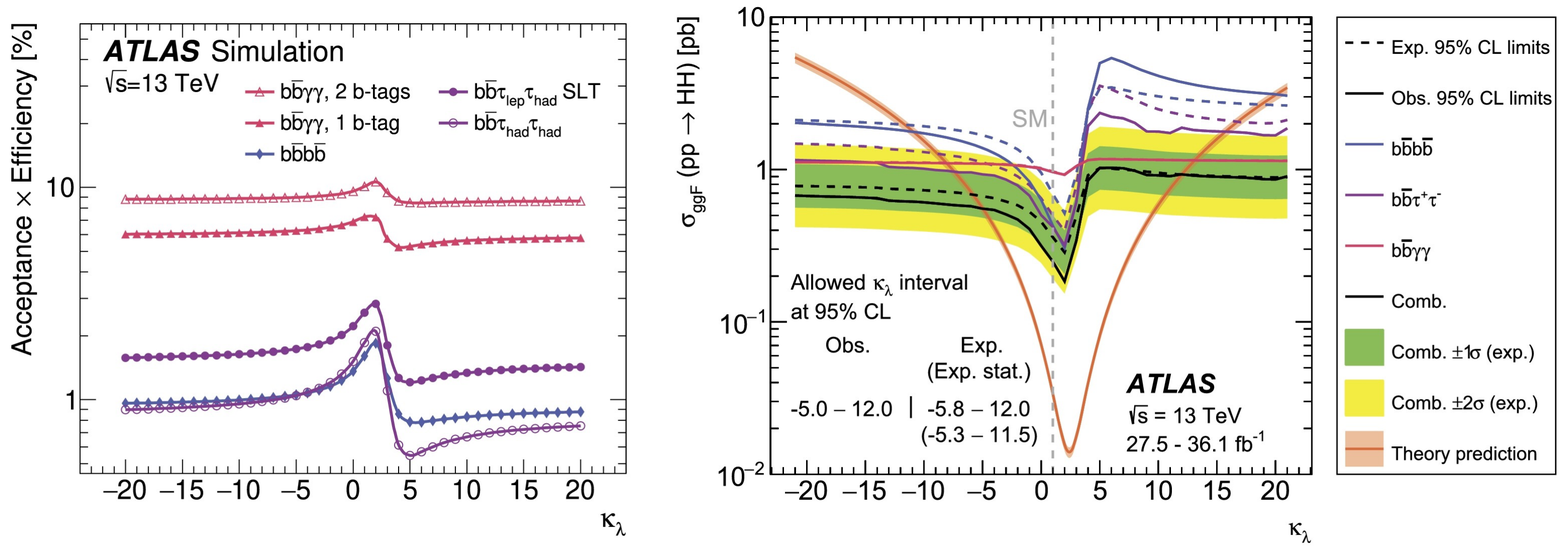

(a) (b)

Fig. 4. (a) Signal acceptance times efficiency as a function of κ_λ for the $b\bar{b}b\bar{b}$, $b\bar{b}\tau^+\tau^-$ and $b\bar{b}\gamma\gamma$ analyses. The $b\bar{b}b\bar{b}$ curve is the average of the 2015 and 2016 curves weighted by the integrated luminosities of the two datasets. (b) Upper limits at 95% CL on the cross-section of the ggF non-resonant SM *HH* production as a function of κ_λ. The observed (expected) limits are shown as solid (dashed) lines. In the $b\bar{b}\gamma\gamma$ final state, the observed and expected limits coincide. The $\pm1\sigma$ and $\pm2\sigma$ bands are only shown for the combined expected limit. The theoretical prediction of the cross-section as a function of κ_λ is also shown. The effect of non-SM Higgs decay branching fractions due to κ_λ variations is not taken into account, which impacts the κ_λ intervals by no more than 7%.

Di-Higgs Combination

Phys. Lett. B 800 (2020) 135103

Table 2
Allowed κ_λ intervals at 95% CL for the $b\bar{b}b\bar{b}$, $b\bar{b}\tau^+\tau^-$ and $b\bar{b}\gamma\gamma$ final states and their combination. The column "Obs." lists the observed results, "Exp." the expected results obtained including all statistical and systematic uncertainties in the fit, and "Exp. stat." the expected results obtained including only the statistical uncertainties. The effect of non-SM Higgs decay branching fractions due to κ_λ variations is not taken into account, which impacts the κ_λ intervals by no more than 7%.

Final state	Allowed κ_λ interval at 95% CL		
	Obs.	Exp.	Exp. stat.
$b\bar{b}b\bar{b}$	$-10.9 - 20.1$	$-11.6 - 18.8$	$-9.8 - 16.3$
$b\bar{b}\tau^+\tau^-$	$-7.4 - 15.7$	$-8.9 - 16.8$	$-7.8 - 15.5$
$b\bar{b}\gamma\gamma$	$-8.1 - 13.1$	$-8.1 - 13.1$	$-7.9 - 12.9$
Combination	$-5.0 - 12.0$	$-5.8 - 12.0$	$-5.3 - 11.5$

Di-Higgs Combination

Phys. Lett. B 800 (2020) 135103

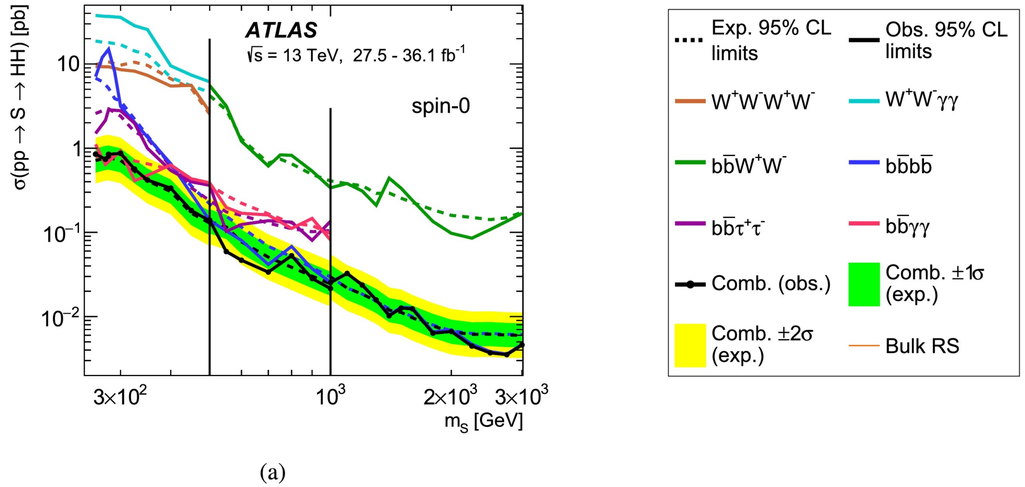

(a)

Fig. 5. Upper limits at 95% CL on the cross-section of the resonant Higgs boson pair production for (a) a spin-0 heavy scalar, (b) a spin-2 KK graviton with $k/\overline{M}_{\mathrm{Pl}} = 1$ and (c) a spin-2 KK graviton with $k/\overline{M}_{\mathrm{Pl}} = 2$. The observed (expected) limits are shown as solid (dashed) lines. The $\pm 1\sigma$ and $\pm 2\sigma$ bands are only shown for the expected limits of the combination. Only the $b\bar{b}b\bar{b}$, $b\bar{b}W^+W^-$ and $b\bar{b}\tau^+\tau^-$ search results are used in the spin-2 resonant combination. The vertical black lines in each panel indicate mass intervals where different final states are combined.

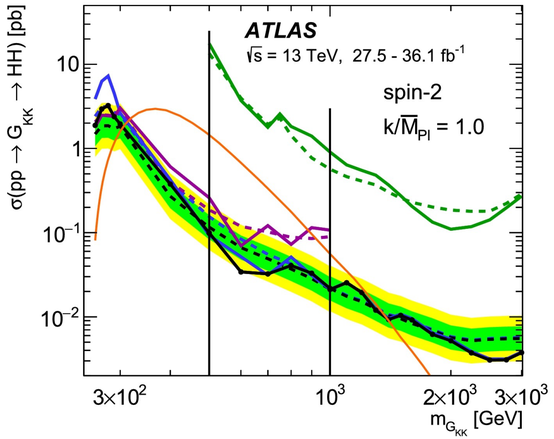

(b)

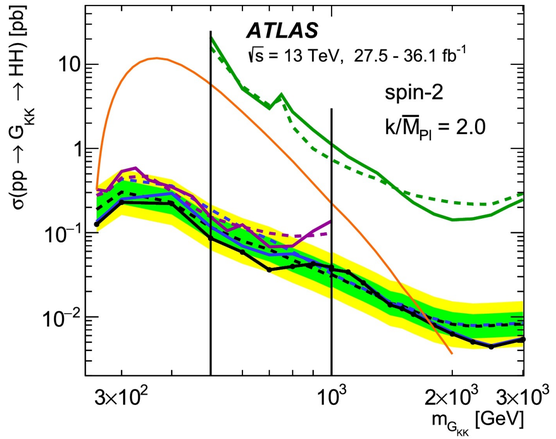

(c)

Di-Higgs Combination

Phys. Lett. B 800 (2020) 135103

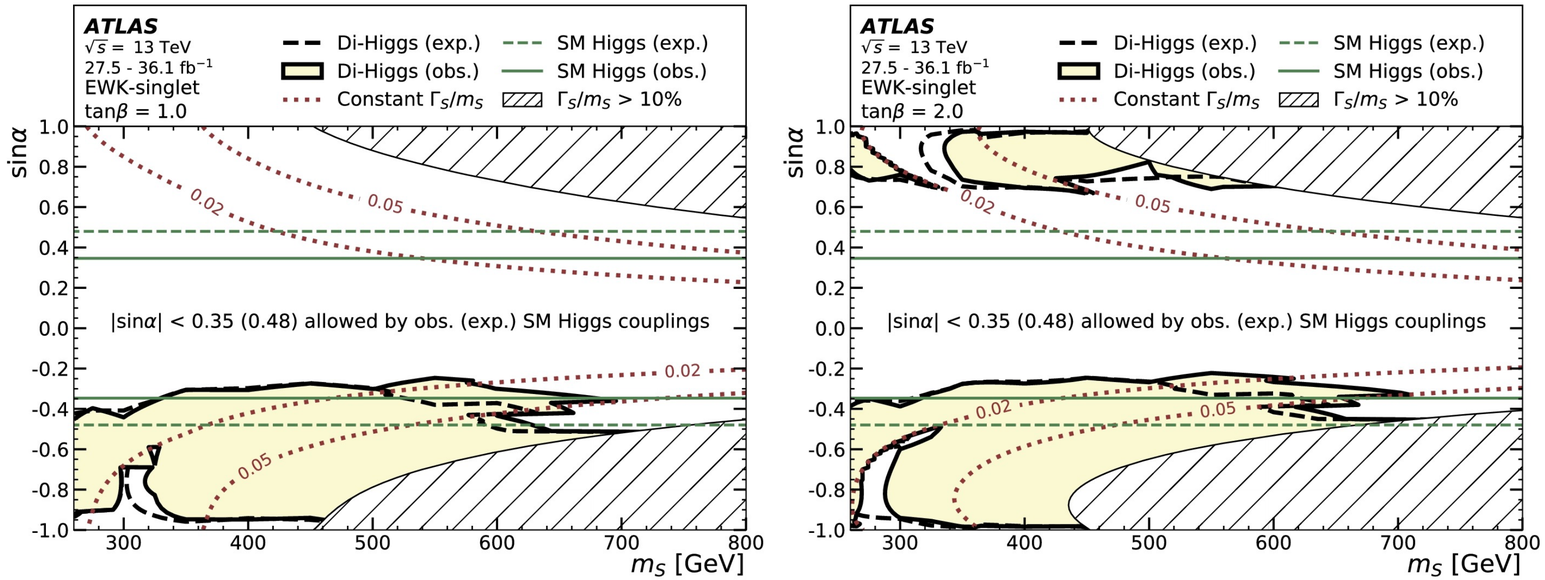

Fig. 6. Excluded regions for the EWK-singlet model for two values of the tan β parameter: (a) tan β=1 and (b) tan β=2. Indirect constraints from SM Higgs coupling measurements [74] are shown with horizontal lines. The dotted lines indicate the separation between regions where the resonance width is larger than 2% and 5% of the resonance mass. The hatch-marked area corresponds to regions that cannot be excluded because the width of the resonance exceeds 10% of the resonance mass, corresponding to the maximum of the experimental mass resolution among all analysed final states.

Di-Higgs Combination

Phys. Lett. B 800 (2020) 135103

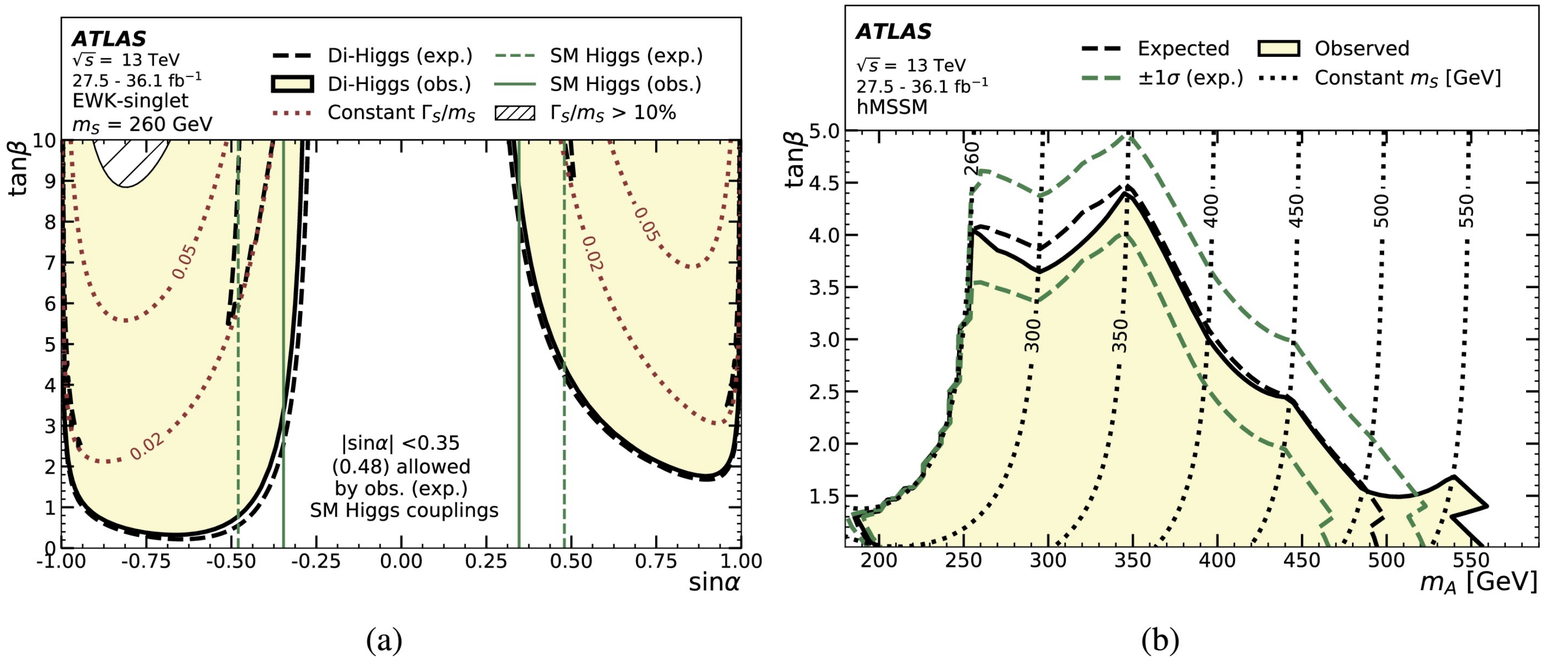

Fig. 7. Excluded regions in (a) the EWK-singlet model for m_S=260 GeV and (b) the hMSSM model using the experimental upper limits obtained in the spin-0 resonance searches. In the EWK-singlet exclusion, the indirect constraints from SM Higgs coupling measurements [74] are shown with vertical lines.

Vector Boson Fusion HH→bbbb

JHEP 07 (2020) 108

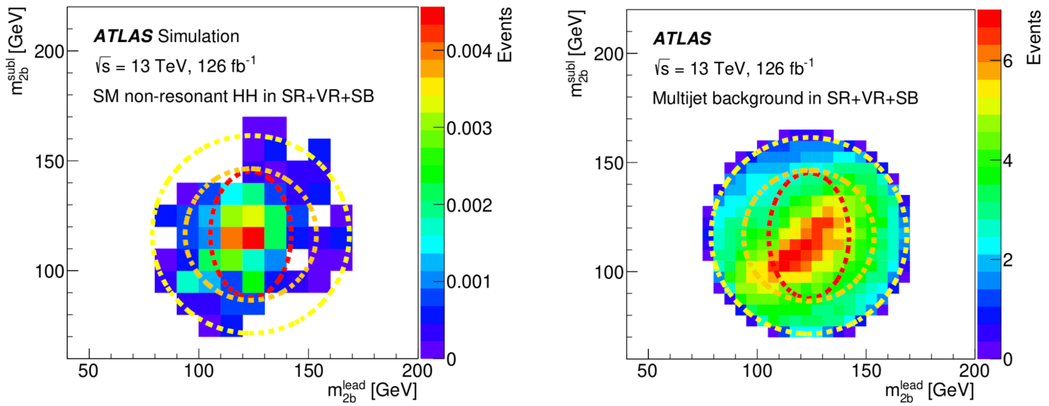

Figure 3. Two-dimensional mass regions used in the analysis. The signal region is inside the inner (red) dashed curve, the validation region is outside the signal region and within the intermediate (orange) circle, and the sideband is outside the validation region and within the outer (yellow) circle. The regions are shown for (a) simulated events from the SM non-resonant HH process and (b) the estimated multijet background.

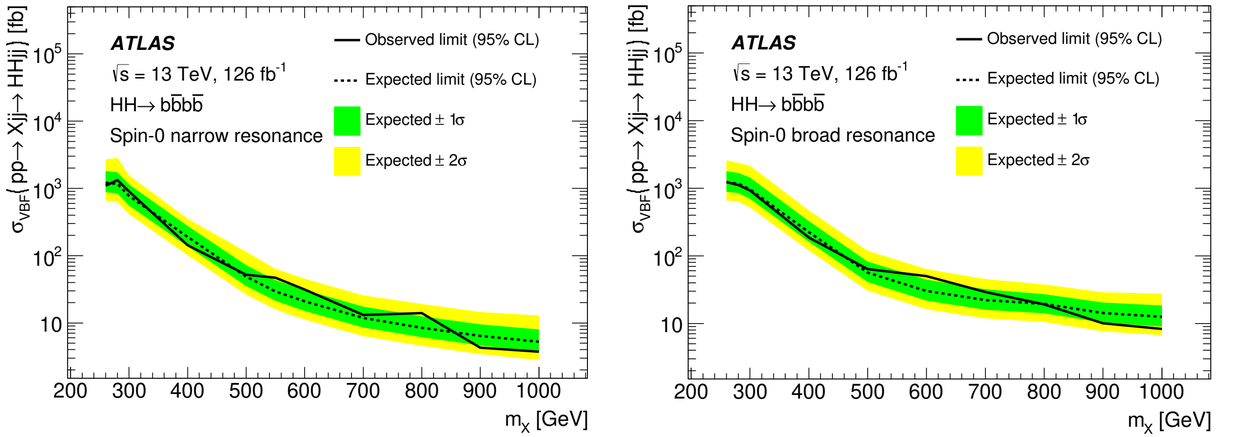

Figure 5. Observed and expected 95% CL upper limits on the production cross-section for resonant HH production via VBF as a function of the mass m_X. The (a) narrow- and (b) broad-width resonance hypotheses are presented.

	Observed	-2σ	-1σ	Expected	$+1\sigma$	$+2\sigma$
σ_{VBF} [fb]	1460	510	690	950	1330	1780
$\sigma_{\text{VBF}}/\sigma_{\text{VBF}}^{\text{SM}}$	840	290	400	550	770	1030

Table 2. Upper limits at 95% CL for SM non-resonant HH production via VBF in fb (first row) and normalised to its SM expectation, $\sigma_{\text{VBF}}^{\text{SM}}$ (second row). Uncertainties related to the branching ratio of the $H \to b\bar{b}$ decay are not considered.

bbℓνℓν Final State

Phys. Lett. B 801 (2020) 135145

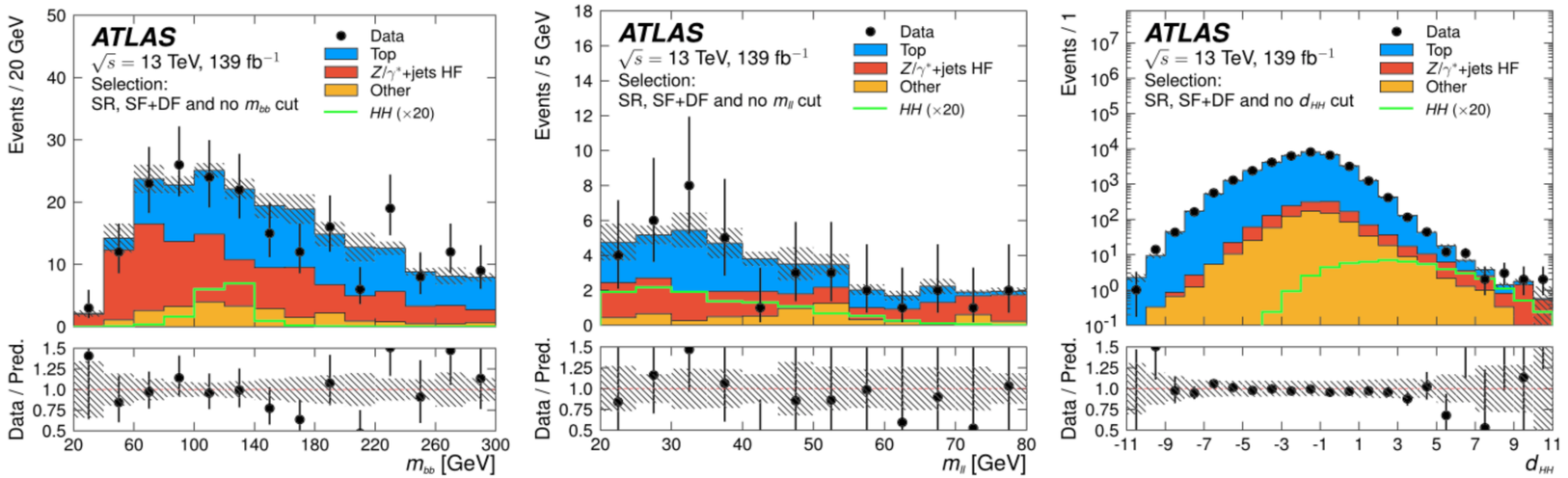

Fig. 3. Distributions of m_{bb} (left), $m_{\ell\ell}$ (middle), and the discriminant d_{HH} (right). The distributions are shown after the fit to data in the control regions under the background-only hypothesis. Each distribution includes both the SF and DF events and imposes signal selection requirements on all quantities except the one being plotted, but the requirement on d_{HH} has been relaxed to $d_{HH} > 5$ for the distributions of m_{bb} and $m_{\ell\ell}$. The $HH \to bb\ell\nu\ell\nu$ signal ("HH") is overlaid and has its cross-section scaled by a factor of 20 relative to the SM prediction for visualisation purposes. The ratio of the data to the sum of the backgrounds is shown in the lower panel of each figure. The hatched bands indicate the combined statistical and systematic uncertainty.

Table 5

Observed and expected upper limits on the ggF-initiated non-resonant HH production cross-section at 95% CL and their ratios to the SM prediction ($\sigma^{\mathrm{SM}}(gg \to HH) = 31.05 \pm 1.90$ fb [13–20]). The $\pm 1\sigma$ and $\pm 2\sigma$ variations about the expected limit are also shown. Uncertainties in the SM cross-section are taken into account when computing the upper limits on the cross-section ratio.

	-2σ	-1σ	Expected	$+1\sigma$	$+2\sigma$	Observed
$\sigma\,(gg \to HH)$ [pb]	0.5	0.6	0.9	1.3	1.9	1.2
$\sigma\,(gg \to HH)\,/\sigma^{\mathrm{SM}}\,(gg \to HH)$	14	20	29	43	62	40

Boosted bbττ Final State

arXiv:2007.14811

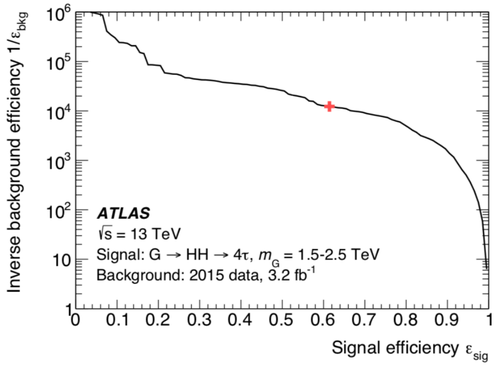

(a)

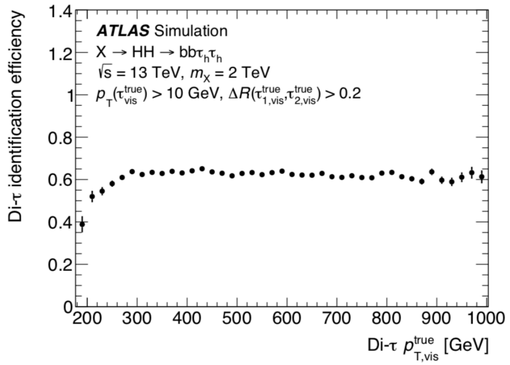

(b)

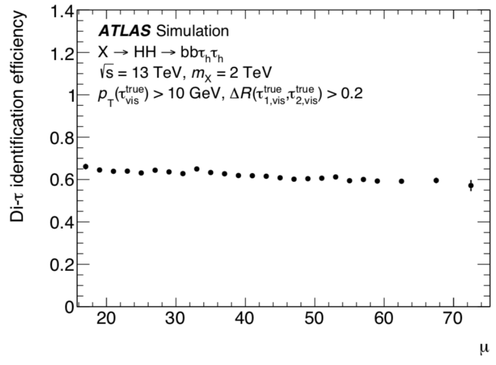

(c)

Figure 3: (a) Background rejection factor versus identification efficiency for the BDT used to discriminate between di-τ signatures and quark- or gluon-initiated jets, as obtained after the di-τ reconstruction step (the red cross indicates the benchmark used in the analysis, corresponding to a signal efficiency of about 60% and a background rejection factor of 10^4), and identification efficiency of boosted di-τ objects, as a function of (b) their p_{T} at generator level and (c) the number μ of pile-up interactions. The vertical error bars only account for statistical uncertainties.

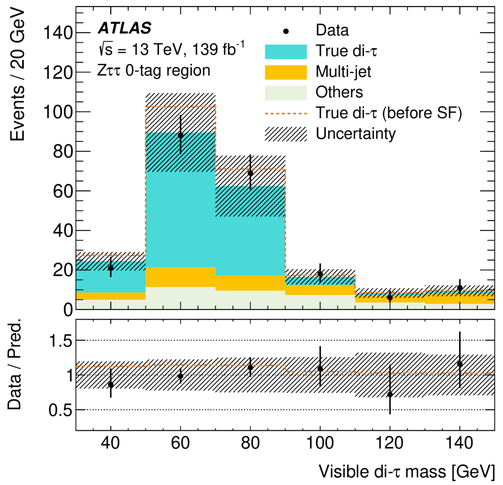

Figure 8: Distributions of (a) the visible mass of the di-τ object, (b) its p_{T} and (c) η in the region labelled as 'Z$\tau\tau$ 0-tag' in Table 2. All simulated events containing a generator-level $\tau^+\tau^-$ pair matched to a simulated di-τ object are referred to as 'True di-τ'. The lower panels show a bin-by-bin comparison of the data and the predicted total background, in terms of event yield ratios. The hatched bands represent combined statistical and systematic uncertainties.

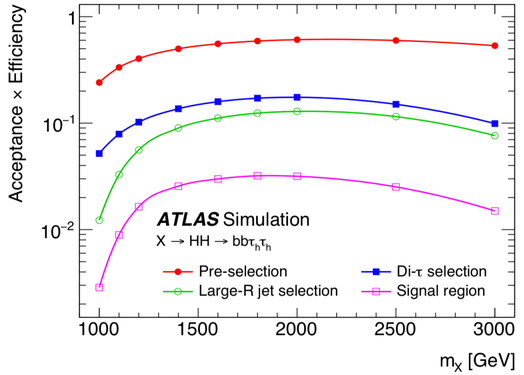

Figure 10: Signal acceptance times selection efficiency as a function of the resonance mass, at various stages of the event selection. From top to bottom: an event preselection (red solid-circle: trigger, object definitions and $E_{\mathrm{T}}^{\mathrm{miss}} > 10\,\mathrm{GeV}$) is performed first; the requirements on the di-τ object and large-R jet detailed in the text are then applied (blue solid-box and green open-circle, respectively); finally, the HH SR definition must be satisfied (pink open-box).